

Wave-Driven Zonal Flow Vacillation in the Southern Hemisphere

DENNIS L. HARTMANN AND FIONA LO

Department of Atmospheric Sciences, University of Washington, Seattle, Washington

(Manuscript received 31 March 1997, in final form 8 September 1997)

ABSTRACT

The variability of the zonal mean flow in the Southern Hemisphere during the period 1985–94 is studied using European Centre for Medium-Range Forecasts analyses. The dominant mode of variability has approximately equivalent barotropic variations of opposite signs centered at 40° and 60°S. This structure is dominant in all seasons and has similar variance in all seasons. The temporal variance of the amplitude of this mode is well modeled as Gaussian red noise with a correlation e -folding time of about 10 days. Zonal wind anomalies are maintained against frictional drag by variations in the zonal flow accelerations driven by transient eddies and associated mean meridional circulations. The eddy structures suggest that equatorward propagation is favored when the jet is displaced poleward and zonal propagation is favored when the jet is displaced equatorward.

1. Introduction

Rossby (1939) introduced the idea of the zonal index cycle to describe the varying strength of the zonal wind and its effect on atmospheric disturbances. Zonally symmetric wind oscillations are not a dominant mode of variability in the Northern Hemisphere where localized jets seem to be more important (Wallace and Hsu 1985), although zonally symmetric modes are the dominant form of low-frequency variability in some model simulations of wintertime Northern Hemispheric flow (e.g., Branstator 1984). The Southern Hemisphere has much weaker stationary planetary wave features, and nearly zonally symmetric variations are the dominant mode of low-frequency variability.

Webster and Keller (1975) and Trenberth (1984) both noted strong intraseasonal and interannual variability of zonal flow in the Southern Hemisphere. Kidson (1988) studied the mean sea level pressure and 500-mb zonal winds in the Southern Hemisphere in Australian analyses from 1968 to 1983. He used correlation analysis and empirical orthogonal functions (EOFs) to show that the primary pattern of variation has anticorrelated centers at 40° and 60°S. The EOF pattern has an equivalent barotropic structure with a frequency dominated by the seasonal and interannual timescales but no obvious periodicities. Nigam (1990) also used EOFs to analyze nine years of global geopotential heights from American and European analyses. He found a dominant EOF struc-

ture in the Southern Hemisphere similar to that of Kidson in both winter and summer. Yoden et al. (1987), Shiotani (1990), and Karoly (1990) further confirmed that the low-frequency variations in the Southern Hemisphere are nearly zonally symmetric and equivalent barotropic. They suggested that fluxes of heat and momentum by transient eddies maintain the variations of zonal mean flow and drive transitions between flow regimes.

Midlatitude zonal flow variability with a structure similar to that observed in the Southern Hemisphere is readily simulated in numerical models. Modeling studies show that low-frequency variations of the midlatitude zonal mean flow can result from forcing by transient eddies. Robinson (1991) showed that low-frequency variability of the midlatitude zonal mean flow was driven by synoptic eddies in a simple two-level model. He found that the zonal flow organizes the eddies to sustain the flow against frictional dissipation. This type of zonal flow variability is similar to the ultralow-frequency variability discussed by James and James (1992), Feldstein and Robinson (1994), and James et al. (1994). Yu and Hartmann (1993) simulated zonal vacillation in a multilevel primitive equation model. The zonal index varied on timescales of hundreds of days and diagnostic studies showed that these long-term variations were maintained by eddy forcing. Composite analysis showed that the synoptic eddies changed their structures in different phases of the vacillation in such a way as to sustain the zonal flow anomalies. During those times when the zonal jet is displaced northward, the composited baroclinic eddy structures show northwest–southeast tilt and mostly equatorward propagation. When the zonal jet is displaced equatorward, the eddies are more banana shaped and seem to propagate more

Corresponding author address: Dr. Dennis L. Hartmann, Department of Atmospheric Sciences, Box 351640, University of Washington, Seattle, WA 98195.
E-mail: dennis@atmos.washington.edu

eastward than equatorward. These structural changes in the eddies are associated with changes in the eddy fluxes that support the zonal flow anomalies. Baroclinic eddy life cycle experiments, started from high and low index zonal flow composites, showed that the eddies acted to enhance the initial zonal flow anomalies even in the presence of realistic forcing and dissipation. These results suggest that the vacillation results from a strong eddy–zonal flow feedback during baroclinic wave life cycles.

Many studies have been performed on the effect of jet structure on baroclinic wave growth and life cycles. Theoretical and numerical studies show that horizontal shear affects baroclinic instability (e.g., McIntyre 1970; James 1987; Dong and James 1997a,b) and that in a quasigeostrophic flow the eddy fluxes of momentum tend to strengthen the jet (Held 1975) unless the jet is narrower than the radius of deformation (Held and Andrews 1983). The direction of eddy momentum flux is quite sensitive to the horizontal shear of the jet (Nakamura 1993; Nakamura and Plumb 1994). Shear also affects the structure of fronts and other subsynoptic features (Davies et al. 1991).

Following up on earlier work by Simmons and Hoskins (1980), Thorncroft et al. (1993) performed a more refined analysis of a particular set of numerical experiments to test the effect of barotropic shear on baroclinic eddy life cycles. This work showed dramatic changes in eddy structure and zonal flow interaction in response to cyclonic barotropic shear. Initial conditions with strong cyclonic barotropic shear give long-lasting undular eddies, while the case without shear gives strong equatorward wave breaking and poleward movement of the westerly jet. Hartmann and Zuercher (1998) showed that, as the initial cyclonic shear is increased from small values to large values, the transition between these two types of life cycle behavior occurs abruptly at a critical value of the barotropic cyclonic shear of the initial zonal flow. Hartmann (1995) noted that the barotropic shear anomaly applied in these idealized experiments is similar in nature to the first EOF of Southern Hemisphere zonal flow variability. By using the amplitude of the first EOF of zonal wind as a compositing index, he showed that the differences in potential vorticity evolution of baroclinic waves in the two extremes of the zonal flow vacillation are similar to those in the idealized life cycle experiments. The sense of these differences is such that the changes in eddy evolution tend to enhance the initial zonal flow anomalies through eddy fluxes of potential vorticity. Lee and Feldstein (1996) showed two types of wave breaking occur in a GCM simulation and that the occurrence of these types of breaking are sensitive to the meridional shear of the flow. Robinson (1996) showed that suppression of barotropic variations of zonal flow greatly decreased the amount of low-frequency variability in his model, suggesting that organization of eddies by the barotropic component of zonal flow is very important in generating

low-frequency variability. Taken together, these elements form a strong case that the quasi-barotropic zonal flow vacillation in the Southern Hemisphere results from the strong feedback between barotropic shear of the zonal wind and the life cycles of baroclinic eddies.

An alternative theory by Feldstein and Lee (1996) holds that impulsive forcing by eddies can drive zonal flow variations that gradually dissipate and that organized feedback between eddies and mean flow is not necessary to produce zonal flow vacillation. Their analysis of an idealized GFDL R30 aquaplanet with no seasonal cycle suggests that fluctuations of their zonal index is excited by impulsive forcing by transient eddy momentum fluxes. In the model they used, the dominant mode of zonal angular momentum is a variation of the subtropical jet and not of a midlatitude eddy-driven jet, so their results are perhaps not directly comparable to the dominant mode in the Southern Hemisphere, which occurs in higher latitudes where the zonal wind is strongly eddy driven.

The purpose of this research is to further study the variations in eddy structure that accompany zonal flow variations in the Southern Hemisphere, using 10 years of ECMWF analyses over the period 1985–94. We will first revisit the EOF analysis of the zonally averaged flow and show that the structure of the first EOF is independent of season. Using the amplitude of this first EOF as an index, we will composite the eddy structure and zonal flow accelerations to show that both the eddy structure and the resulting zonal flow accelerations act to sustain the zonal flow anomalies. Composited eddy correlation structures will be investigated to see if the differences are similar to those found in numerical simulations.

2. Data and EOF analysis

The European Centre for Medium-Range Weather Forecasts assimilated dataset used in this study covers the period from 1 January 1985 to 31 December 1994. Analyses are performed on Southern Hemisphere temperature and winds taken daily at 0000 UTC. The grid resolution is 2.5° in both longitude and latitude at 10 vertical pressure levels: 1000, 850, 700, 500, 400, 300, 250, 200, 150, and 100 mb. Kidson (1988) and Karoly (1990) showed that the leading modes of low-frequency variation in the Southern Hemisphere troposphere are nearly zonally symmetric. For this reason we feel justified in performing a zonal average before doing the EOF analysis.

One remarkable characteristic of the Southern Hemisphere zonal flow is the modest seasonal variation of the midlatitude tropospheric jet compared to that in the Northern Hemisphere. Figure 1 shows the monthly mean zonal wind averaged over the 10-yr sample. All months show a midlatitude jet with surface westerlies between 40° and 60°S . At upper levels, the subtropical jet near 30°S shows a strong seasonal variation with the strong-

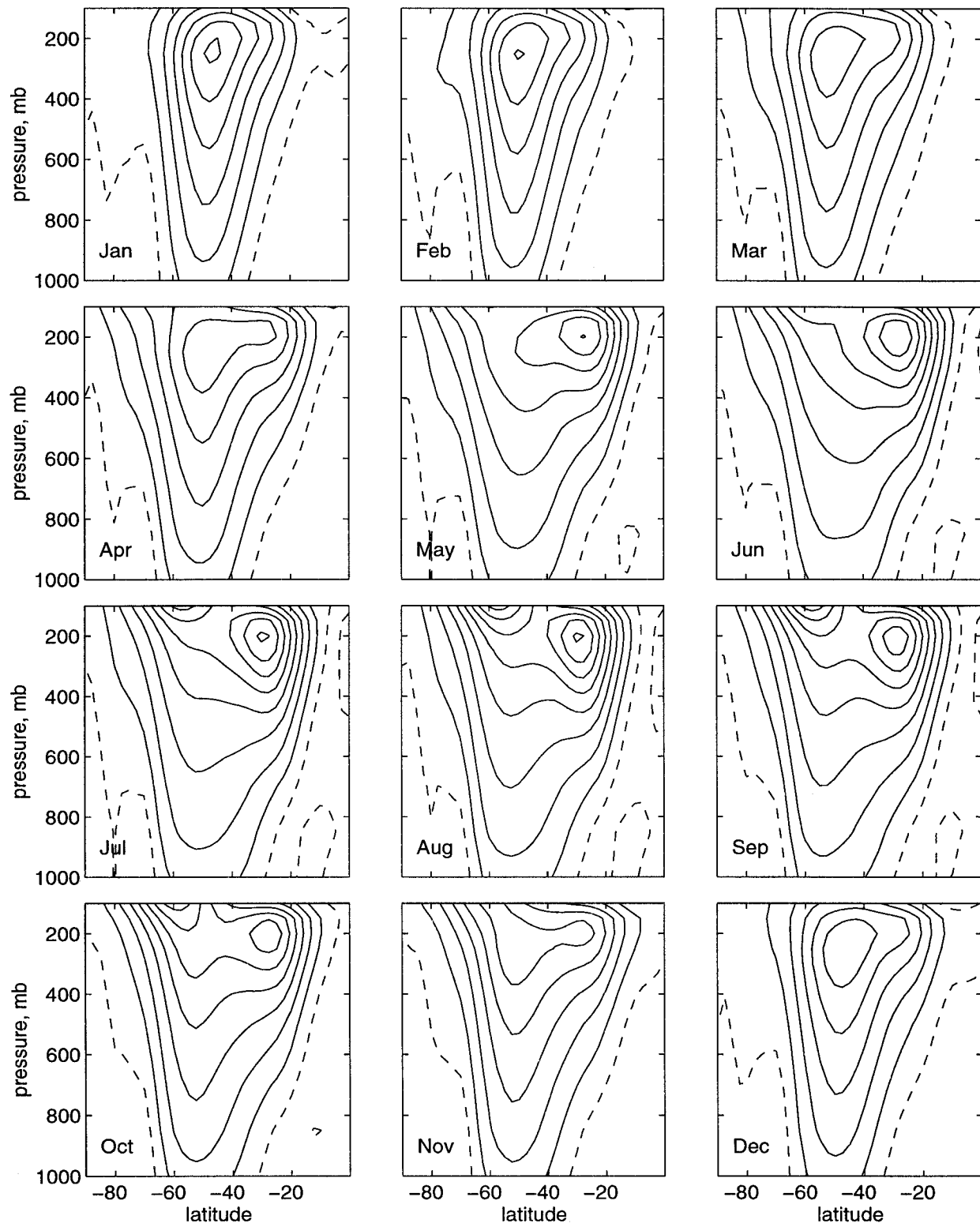


FIG. 1. Monthly mean zonally averaged zonal wind for the period 1985–94. Contour interval is 5 m s⁻¹. The zero and negative contours are dashed.

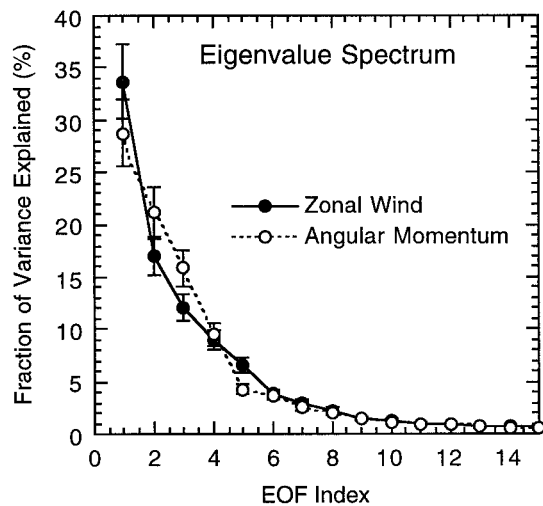


FIG. 2. Eigenvalue spectra for EOF analysis of zonal mean wind and zonal mean angular momentum with error bars.

est subtropical jet in July and August when the Hadley circulation transports angular momentum southward at upper levels in the Southern Hemisphere (Peixoto and Oort 1992). The seasonal variation of the eddy-driven midlatitude jet appears much less pronounced.

The annual cycle is first removed from the daily zonal mean wind data. The annual cycle is calculated by averaging the 10 years of data for each calendar day and then putting this mean annual cycle through a 20-day low-pass filter to remove sampling noise. After removing the annual cycle, a 10-day low-pass filter is applied to the time series of zonal-mean zonal wind anomalies before performing the EOF analysis. This filtering does not affect the resulting EOF structures much because the zonal average anomalies tend to vary on longer timescales. Low-pass filtering of the input data has little effect on the dominant structures but does increase the fraction of variance explained by them.

EOF analysis of both the zonal wind anomalies and the zonal angular momentum anomalies was performed. The eigenvalue spectra for these two analyses have a somewhat similar shape, but the first EOF is more dominant for the zonal wind (Fig. 2). For zonal wind the first five eigenvalues pass the North et al. (1982) test for explaining a distinct fraction of variance. The first four eigenvalues for angular momentum decrease almost linearly and pass the North et al. test, and then the spectrum abruptly becomes a continuum of indistinct eigenvalues. From this comparison we infer that the first eigenvalue is less unusual in the angular momentum analysis than in the zonal wind analysis, and this relates to its poleward location. From a dynamical perspective, angular momentum is probably a more meaningful quantity since it is conserved for ideal flows.

The first three EOFs of zonal mean wind and angular momentum are shown in Fig. 3. The structures of the first modes of zonal wind and zonal angular momentum

are similar to each other. This is the same first mode seen in previous observational studies and in the modeling studies of Robinson (1991) and Yu and Hartmann (1993). It has centers of opposite polarity at about 40° and 60°S and is approximately equivalent barotropic. This mode of variability explains a larger fraction of the variance of zonal wind (34%) than of angular momentum (29%) because of its more poleward position. For higher EOFs more difference appears between the wind and angular momentum structures, with the angular momentum structures increasingly concentrated in low latitudes. In this study we will consider only the first EOF and use the zonal wind as our compositing standard. This will focus attention on the eddy-driven midlatitude jet and its variations. A focus on the higher modes of the angular momentum analysis would undoubtedly bring in more influence from the tropical circulation and associated variations in the subtropical jet and Hadley circulation. The second EOF of angular momentum might be a good basis for studying the interaction between the subtropical jet and the midlatitude jet.

Most studies of midlatitude dynamics have concentrated on the winter season. In the Southern Hemisphere the eddy-driven vacillation in middle latitudes has a similar structure and importance in all seasons. Figure 4 shows the structure and fraction of explained variance of the first EOF of zonal wind for each of the four traditional 3-month seasons. The structure and fraction of variance explained are remarkably similar in all seasons. The absolute amount of variability explained by this mode is also almost independent of season. Figure 5 shows the variance of the daily principal component (PC1, projection coefficient) of the all-season EOF shown in Fig. 3a within each calendar month of the year, averaged over our 10-yr sample. The first EOF was projected on the 10-day low-pass filtered data to make this plot. While we observe variability from month to month, which may be related to sampling variations, significant variability in the amplitude of the first EOF mode is present in all months. Because the first EOF is present in all seasons with the same structure, we will perform further analysis without seasonal stratification, which greatly increases our sample size and simplifies the analysis.

We can now project the first EOF structure on the unfiltered zonal wind and investigate its temporal variability. A histogram of the daily principal component is shown in Fig. 6. Its histogram is almost Gaussian but is slightly negatively skewed. About 313 days are more than 1.5 standard deviations below the mean value, while only 189 are 1.5 standard deviations above it. The zonal wind structure spends more time in the low index phase than in the high index phase. The mean duration is 6.2 days for a high index event and 8.6 days for a low index event. Thus, when the jet is shifted equatorward, it tends to remain there longer than when it is shifted poleward. This is the same sense as the stronger

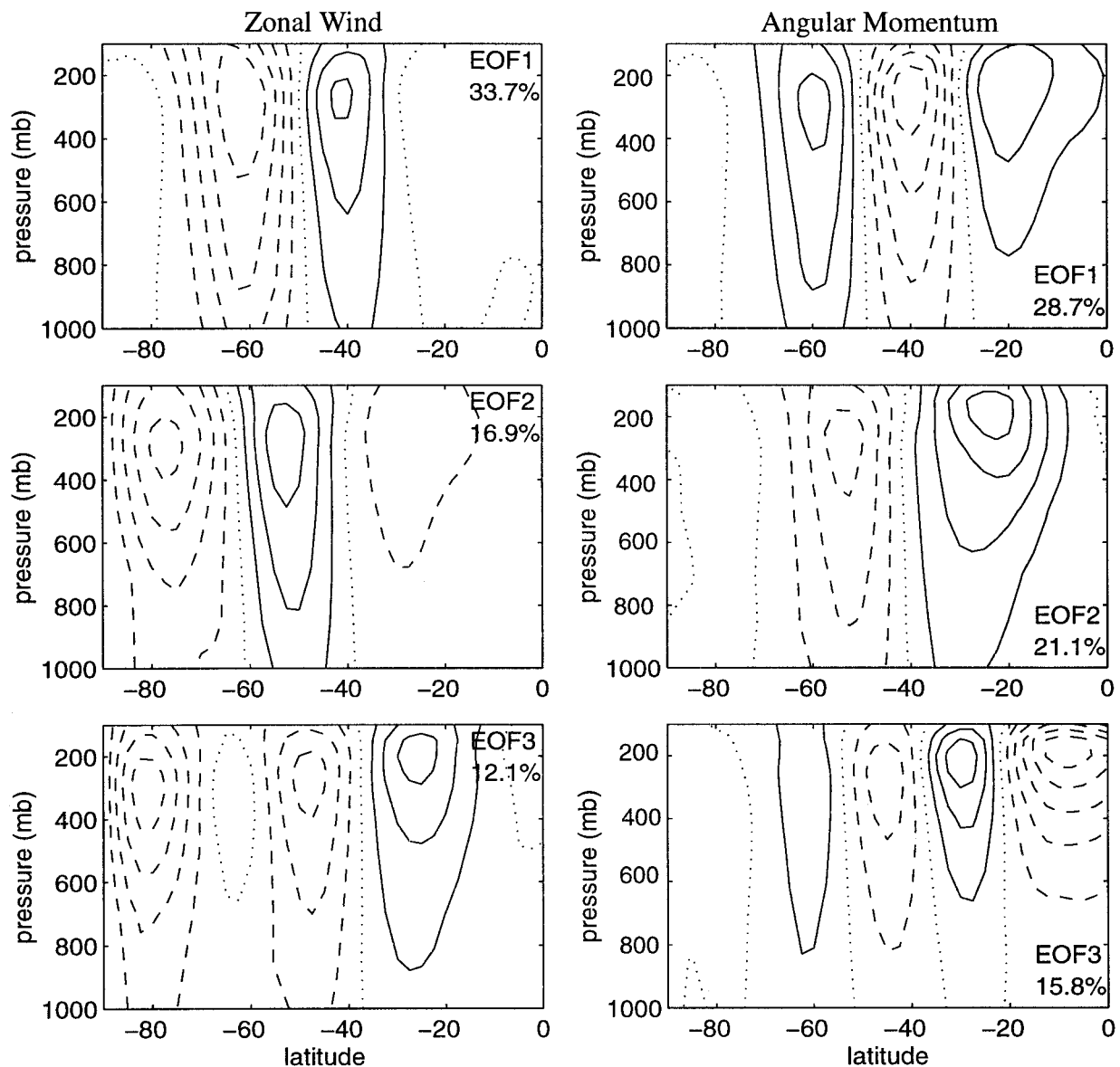


FIG. 3. First three EOFs for zonal wind (left) and angular momentum (right). Explained variance is given in percent in each panel. Dashed contours are negative, zero contour is dotted.

skewness described by Robinson (1991) for his model results, which showed more extreme departures with westerly anomalies at 40° and easterly anomalies at 60° latitude than for anomalies of the opposite sense. Westerly anomalies at 40° and easterly anomalies at 60° give cyclonic zonal mean shear anomalies.

The timescale of the variations are illustrated with a power spectrum of the principal component of the first EOF projected on the unfiltered zonal wind (Fig. 7). This spectrum has a bandwidth of 0.002 cycles per day and at least 15 degrees of freedom. The power spectrum is statistically indistinguishable from that of red noise with an autocorrelation at one day of about 0.8. That is, we cannot reject a null hypothesis that it is red noise

at the 99% a priori significance level. Therefore, almost Gaussian red noise is a good model for the temporal variability in the EOF structure. We cannot make a case for bimodality or periodicity, although slight skewness is evident. The autocorrelation has an e -folding time of about 10 days for the unfiltered data used in this analysis. The redness of the spectrum for zonal flow variations in models was discussed by James and James (1992) and Feldstein and Robinson (1994).

3. Composites and momentum budget analysis

We construct composites by averaging those days during which the amplitude of the first EOF projected on

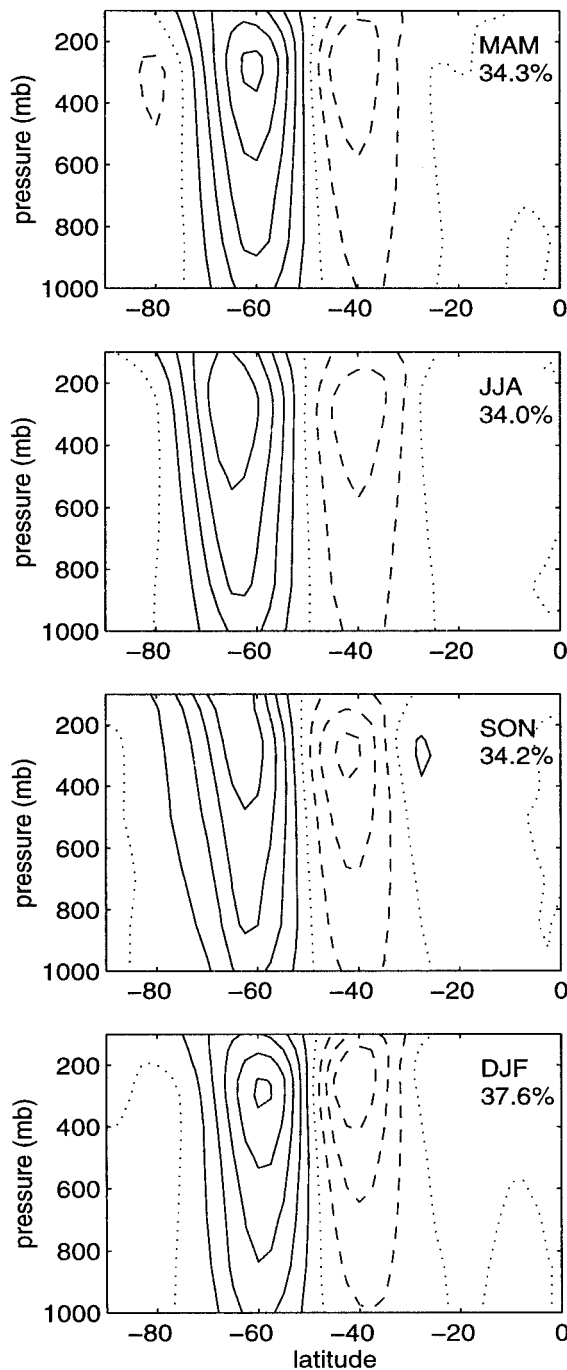


FIG. 4. First EOF of 10-day low-passed zonal mean wind for four seasons; otherwise as in Fig. 3.

the zonal mean wind anomaly is 1.5 standard deviations above or below its mean value. Composite plots of the zonal wind anomalies and eddy flux properties provide information on the eddy–zonal flow interaction. The positive composite is called the high index because the strongest winds are in high latitudes and the low index case is the more cyclonic, low-latitude jet. We have done these composites for annual data as well as for each

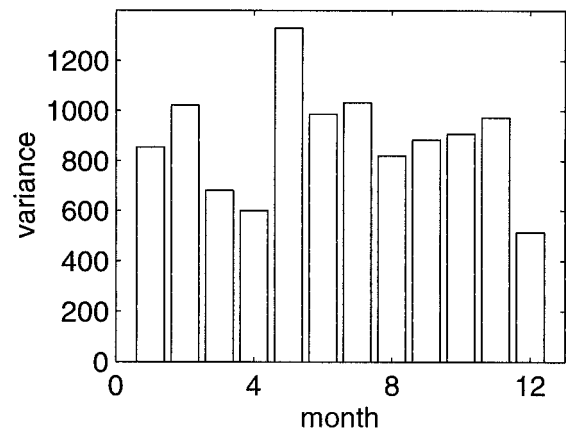


FIG. 5. Variance of the amplitude of the first EOF (PC1) within each month of the year.

individual season (Lo 1996), but we show here only the annual results including all seasons. The seasonal results are quite similar, despite the significant annual cycle in the strength of the subtropical jet.

Zonal-mean zonal wind composites have distinct wind structures for the high and low index phase (Fig. 8). The high index composite shows a jet with dual maxima in the upper troposphere. The winds peak at a value of 32.6 m s^{-1} at 62.5°S at 200 mb, and the secondary jet is slightly weaker with a peak of 30 m s^{-1} at 30°S . At the surface, the westerly jet has a maximum of 10 m s^{-1} at 55°S . The low index is characterized by a single broad jet of slightly greater peak winds of 33.2 m s^{-1} at 200 mb and 42.5°S . The surface maximum wind speed for the low index phase is 7.7 m s^{-1} at 47.5°S . The surface westerly maximum is about 10° farther equatorward in the low index composite. The difference in wind speed peaks at about 300 mb and is more than 10 m s^{-1} at both 40° and 60°S , although relative changes are larger near the surface. At low levels the zonal wind variations associated with the first

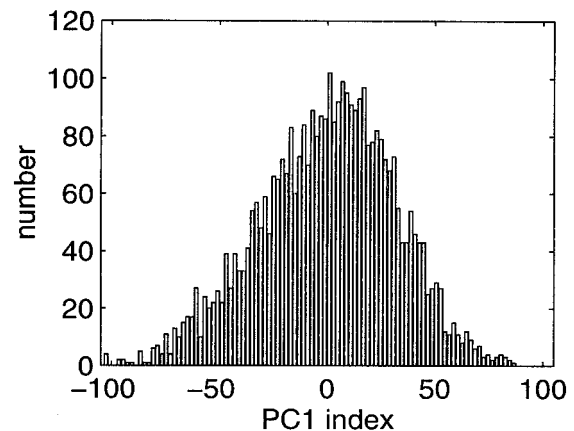


FIG. 6. Histogram of the amplitude of the first EOF of zonal wind projected on the unfiltered data.

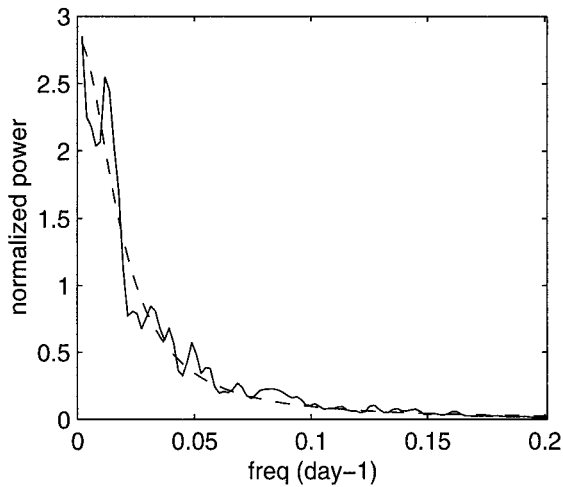


FIG. 7. Averaged power spectrum of the time series of the amplitude coefficients of the first EOF projected onto the unfiltered zonal wind (PC1). Dashed line is the best-fit red noise power spectrum.

EOF are larger than the seasonal variations. Differences between the 1.5 standard deviation anomaly composites are as large as the seasonal variations (not shown).

To understand the interaction of eddies with mean zonal wind in the zonal flow vacillation, the forcing of zonal flow tendency in each extreme phase of the vacillation is studied using transformed Eulerian mean (TEM) diagnostics of the zonal momentum balance (Edmon et al. 1980):

$$\begin{aligned} & \frac{\partial}{\partial t} [u] \cos \varphi \\ &= f[v^*] \cos \varphi + \frac{1}{r \cos \varphi} \frac{\partial}{\partial \varphi} \{ -[u'v'] \cos^2 \varphi \} \\ & \quad + \frac{\partial}{\partial p} \left\{ f \frac{[v'\theta']}{\partial/\partial p[\theta]} \cos \varphi \right\} + F_x \cos \varphi. \end{aligned} \quad (1)$$

Brackets, $[x]$, denote a zonal mean of the field x ; primes, x' , denote departures from zonal mean; and u is zonal wind, v is meridional wind, θ is potential temperature, r is the radius of the earth, φ is latitude in radians, and f is the Coriolis parameter. Here $[v^*]$ is the residual meridional velocity:

$$[v^*] = [v] + \frac{\partial}{\partial p} \left\{ \frac{[v'\theta']}{\partial/\partial p[\theta]} \right\}. \quad (2)$$

The first term on the right-hand side of (1) is the acceleration of the zonal wind associated with the Coriolis acceleration by the residual circulation. The second term containing the meridional eddy momentum flux will be called the barotropic part of the eddy forcing. The third term is related to the eddy heat flux and will be called the baroclinic part of the eddy forcing in which F_x is the zonal component of frictional drag. The sum of the first three terms on the right-hand side of (1) is defined

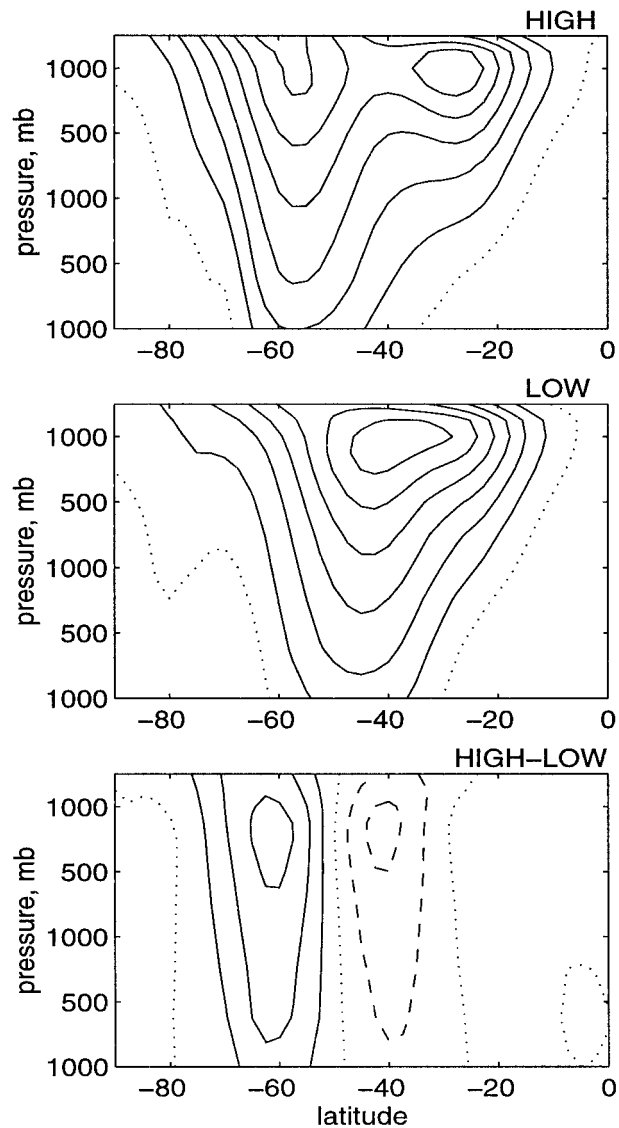


FIG. 8. Zonal mean wind of high index composite, low index composite, and the high composite minus the low composite. Contour interval is 5 m s^{-1} , dotted line is zero contour, and dashed lines are negative.

as the net advective forcing and is the acceleration that would be produced in the absence of subgrid-scale momentum forcing.

Pfeffer (1987) has questioned the usefulness of the TEM formulation of the momentum balance, but we prefer it here for several reasons: We wish to show the relative importance of eddy momentum flux and eddy heat flux in driving zonal flow accelerations and to show that large changes in these fluxes occur that support the changed zonal flow during the zonal flow vacillation. In the TEM equations the meridional eddy momentum flux convergence and the total advective forcing are unchanged from their traditional Eulerian descriptions, but the acceleration by the Eulerian meridional circu-

lation that is driven by eddy heat flux convergence is moved to the baroclinic eddy forcing term in the zonal momentum equation. The sum of the barotropic and baroclinic eddy forcing terms is just the quasigeostrophic potential vorticity flux. Thus, a direct and informative comparison of the relative roles of eddy momentum flux and eddy heat flux is achieved with the TEM formulation. Randel (1990) used the TEM formulation to investigate relationships between transient eddy forcing and accelerations of zonal flow in the Northern Hemisphere.

Figure 9 has 15 panels that show the time mean barotropic, baroclinic, Coriolis, net advective forcing for the high and low index composites, and their difference. The top three panels show the eddy barotropic forcing of the zonal momentum. The forcing is relatively small compared to the other components that force the mean flow, but the difference between the high and low composites is of significant magnitude. The barotropic forcing in the high composite forms a dipole in the upper troposphere associated with poleward eddy momentum flux, but in the low composite three centers of forcing appear that are associated with convergence of momentum from both north and south. The difference plot indicates a more intense poleward eddy momentum flux across 50°S when the jet is displaced northward, giving westerly acceleration at 60°S and easterly acceleration at 40°S.

The baroclinic eddy forcing provides westerly acceleration near the surface and easterly acceleration near the tropopause (second row of Fig. 9). The magnitude of this effect is larger than the barotropic term, but the difference between the two composites is similar in magnitude to the difference in the barotropic eddy forcing. The sum of the two eddy forcing terms (third row of Fig. 9), which is equivalent to the Eliassen–Palm flux divergence, shows a difference plot with the strong dipole structure in the upper troposphere seen for the barotropic term. The net eddy forcing in the upper troposphere is nearly canceled by the Coriolis acceleration associated with the residual circulation (fourth row of Fig. 9), and the net advective forcing (fifth row) is small in the upper troposphere compared to its large values near the surface. Near the surface the net advective forcing shows a large residual, which is required to balance the change in surface drag and keep the anomalous zonal winds in balance. It provides westerly acceleration anomalies where the surface wind anomalies are westerly and easterly accelerations where the anomalous surface wind is easterly (compare with the wind anomaly shown in Fig. 8). In this way large anomalies of surface zonal wind can be maintained for long periods of time, even in the presence of strong surface drag, because the eddy fluxes and associated residual circulation change with the zonal flow to maintain momentum balance. These budget differences are very similar to those shown in the numerical model of Yu and Hartmann (1993).

This analysis of the anomalous zonal angular momentum budget shows that the eddy forcing occurring in both the lower and upper troposphere corresponds to the 40°–60°S alternating structure of EOF1. The eddy heat and momentum forcings are distinctly different for the high and low index phase of the zonal flow vacillation. This strong coupling between of zonal flow and eddy forcing supports the hypothesis that the eddies are organized to support the anomalous zonal winds associated with the zonal flow vacillation. It is consistent with modeling work of Robinson (1991), who showed that the eddy forcing and the zonal wind anomalies varied in phase with each other on longer timescales.

4. Eddy structure composites

Results shown in the previous section indicate that the transient eddy fluxes of heat and momentum are significantly different for the extreme phases of the zonal flow vacillation. This section analyzes the structure of the eddies in the different phases of the zonal index cycle using spatial correlation maps. Yu and Hartmann (1993) used one-point correlation maps to show changes in eddy structures in the different phases of the index cycle in their model. They found distinct eddy structures in the high and low index phases. During the high index periods eddies tilted in the northwest–southeast direction, indicating strong equatorward propagation (Hoskins et al. 1983), while during the low index periods the eddies were more banana shaped and showed more coherent structure in the zonal direction, suggesting a stronger zonal waveguide.

To examine the structure of eddies, we use composite one-point correlation maps of relative vorticity at 300 mb. The one-point correlation composites are generated by first finding the relative vorticity for a spherical coordinate system from the zonal and meridional winds. To minimize noise and focus on the baroclinic life cycles, the time series is bandpass filtered to retain variance with periods between 2.5 and 10 days. It is these periods that contribute most to the changes in eddy fluxes (not shown). The relative vorticity at every point is correlated with the time series of relative vorticity at a reference latitude and reference longitude on the same day. The reference point is shifted through all longitudes and these maps are composited to make one map that represents the data at all longitudes. For the ECMWF 2.5° data, 144 one-point correlation maps are created for each reference latitude. Each of these correlation maps are rotated to a common reference longitude and the results combined, so that the correlations are a composite of all longitudes at each latitude shown.

Figure 10 shows the 300-mb one-point correlation composites for bandpassed relative vorticity with reference latitudes at 40°, 45°, 50°, and 55°S for the high and low index composites. The correlation pattern is tilted NW–SE for the high index composite, suggesting strong equatorward propagation. The correlation pattern

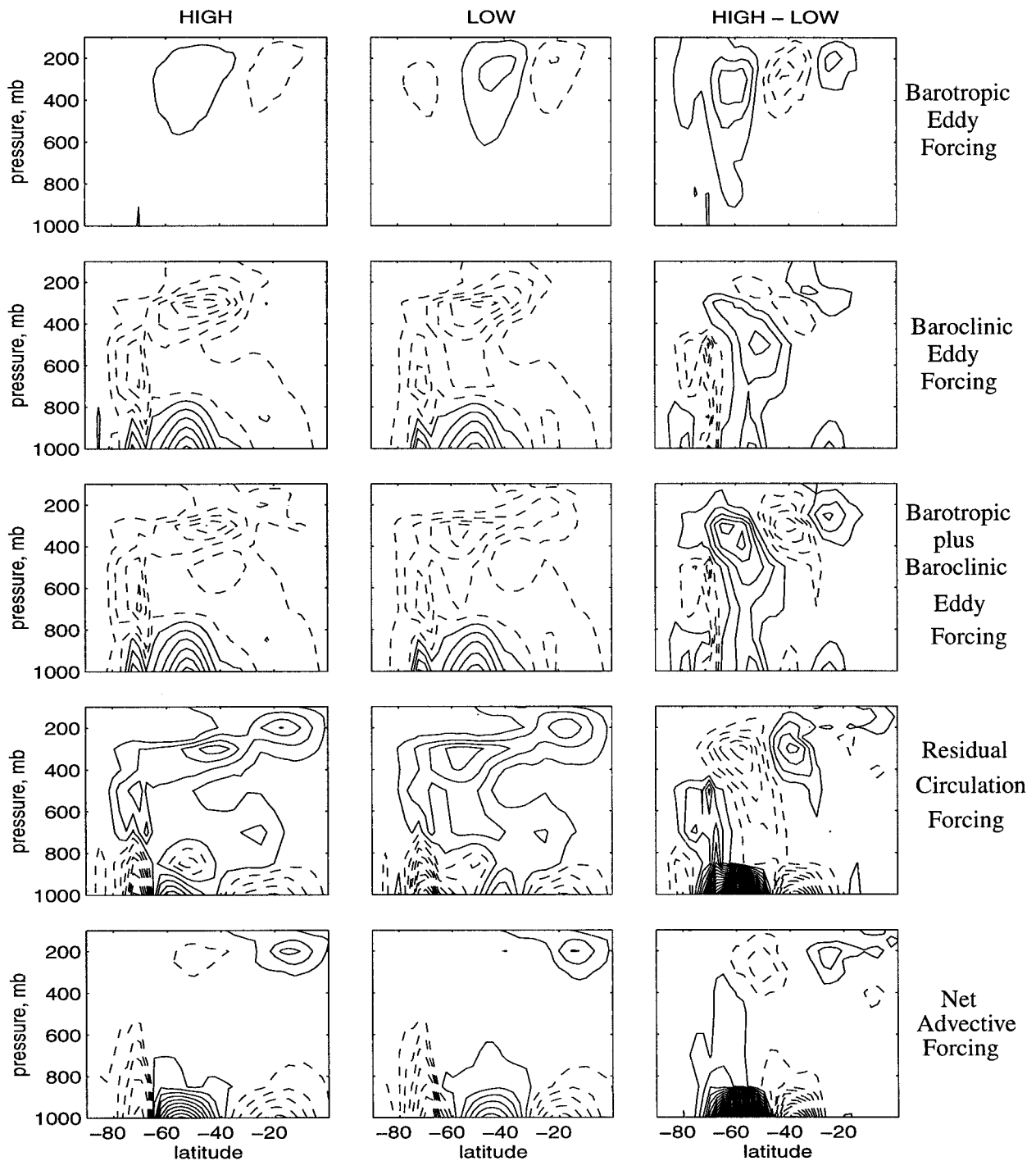


FIG. 9. Transformed Eulerian mean momentum balance for the high index composite (left column), low index composite (center), and high minus low difference (right). Terms are defined in text. Contour interval for composites is $1.5 \text{ m s}^{-1} \text{ day}^{-1}$ and for difference plots is $0.4 \text{ m s}^{-1} \text{ day}^{-1}$. Solid contours indicate a westerly acceleration and dashed lines an easterly acceleration. The zero contour is omitted.

for the low index composite shows a more N-S orientation, indicating less equatorward propagation and more eastward propagation. The low composite shows more banana-shaped structures, and at the highest latitudes we see evidence of poleward propagation in the

NE-SW tilt of the correlation centers. In both composites one can see evidence of an equatorward path and a zonal path for the correlation pattern, but the zonal path is favored in the composite with the more equatorward jet and the equatorward path is favored when

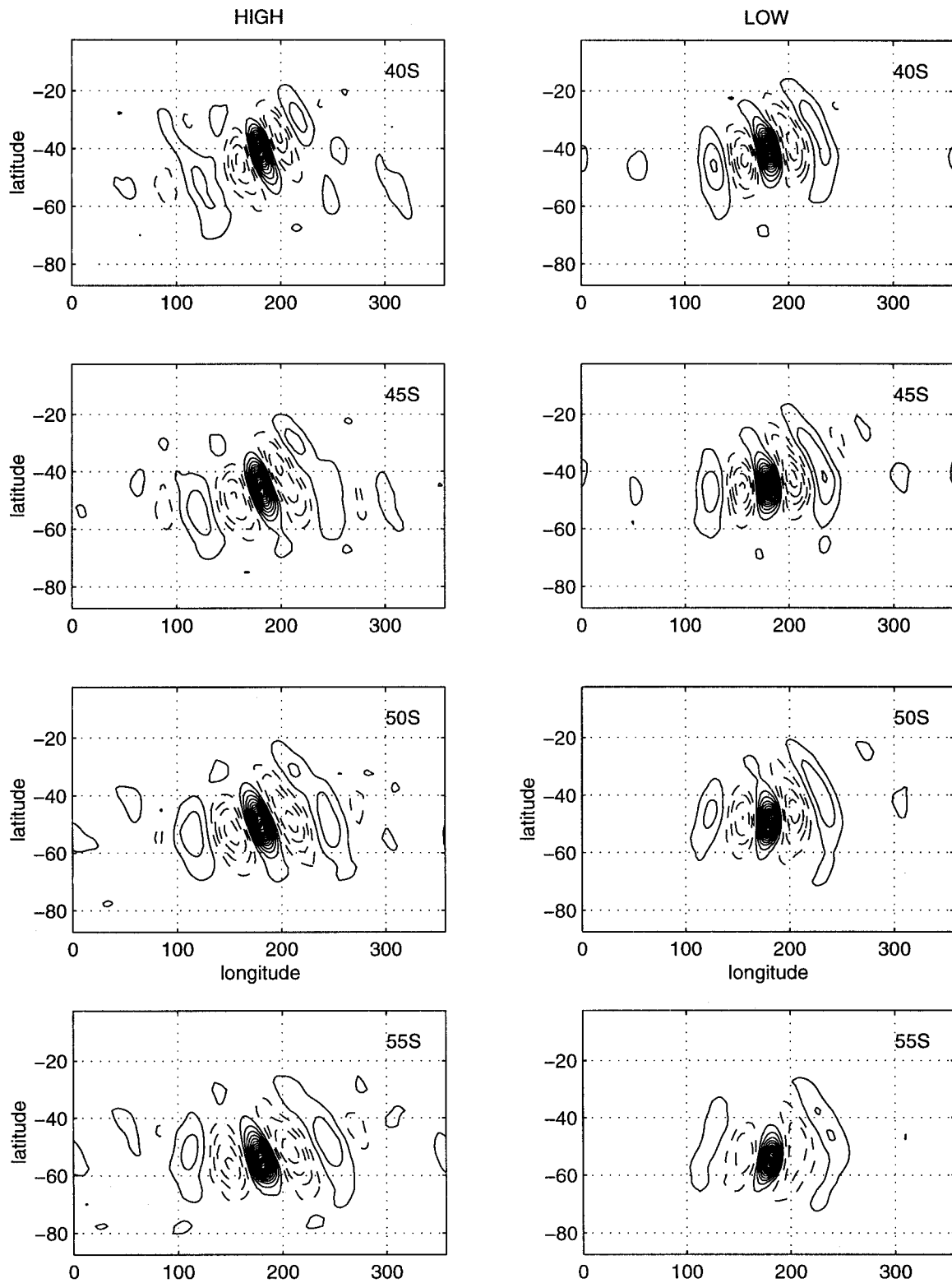


FIG. 10. Simultaneous correlation maps of 2.5–10-day bandpassed relative vorticity at latitudes of 40°, 45°, 50°, and 55°S for the high index periods (left column) and the low index periods (right). The contour interval is 0.1, negative contours are dashed, and the zero contour is omitted.

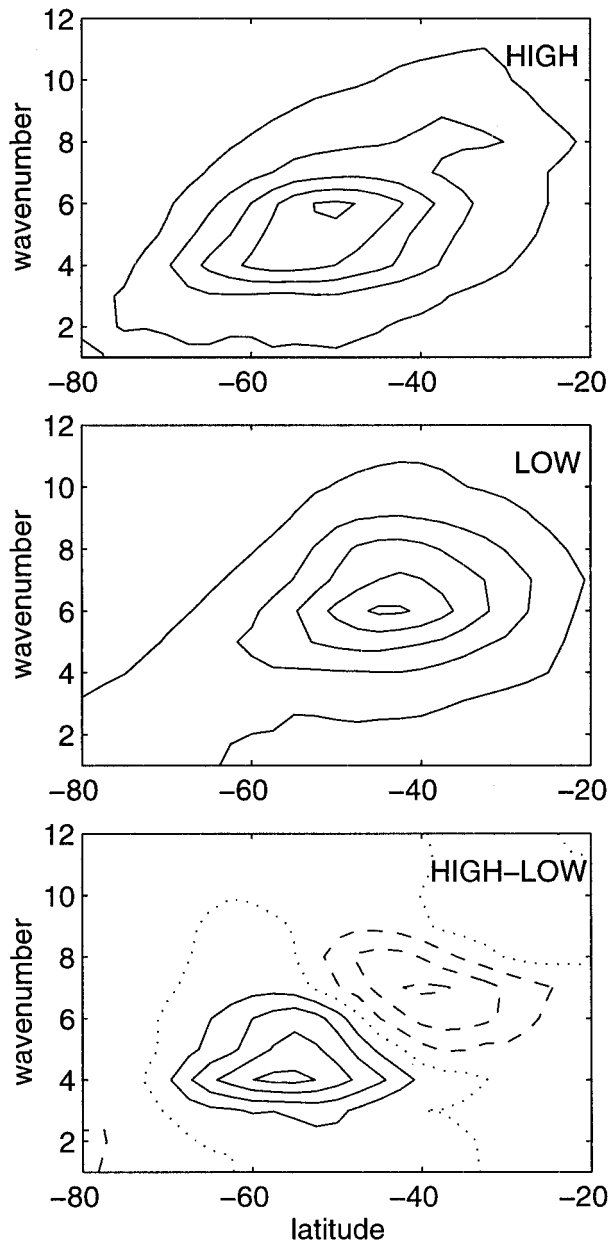


FIG. 11. Ten-day high-passed eddy kinetic energy as a function of latitude and zonal wavenumber for the high and low index periods and the difference between them. The contour interval is $5 \text{ m}^{-2} \text{ s}^{-2}$ for the composites and $3 \text{ m}^{-2} \text{ s}^{-2}$ for their difference. Negative differences are dashed and the zero contour is dotted.

the jet is displaced poleward. These differences are similar to, although less pronounced than, the differences shown in Yu and Hartmann's model study.

The distribution of the 10-day high-passed eddy kinetic energy as a function of latitude and zonal wavenumber for the high and low composites is shown in Fig. 11, along with the difference between the two composites. The high-frequency eddy kinetic energy moves north and south with the jet in the lower troposphere.

The change in zonal wavenumber is about what would be observed if the eddies maintained a constant zonal scale as they shift poleward. Balancing zonal vorticity advection against the beta effect

$$[u] \frac{\partial \zeta}{\partial x} \approx \beta v \quad (3)$$

and assuming that the zonal wind strength and jet shape are invariant and the waves are isotropic gives the scaling that the zonal wavenumber, m , should vary as $m \approx \cos^{3/2} \varphi$, which is about the right scaling to explain the shift from $m = 7$ at 40°S to $m = 4$ at 60°S as suggested in the difference plot in Fig. 11. It is difficult to distinguish, however, between this interpretation and the interpretation that the eddies just retain the same physical wavelength as they move into high latitudes, which requires $m \approx \cos \varphi$. The length scale implied by (3) is the energy cascade "arrest" scale discussed by Rhines (1975) and is also the scale for which baroclinic eddy life cycles attain the largest energy (e.g., Gall 1976; Simmons and Hoskins 1980; Hartmann and Zuercher 1998).

5. Conclusions

This study of the ECMWF observational analysis of the Southern Hemisphere during 1985–1994 has confirmed several aspects of our understanding of zonal flow vacillation in the Southern Hemisphere and its interaction with baroclinic eddies.

- The dominant mode of low-frequency variability is an equivalent barotropic vacillation of the zonal mean wind with centers of opposite sign near 40° and 60°S . This structure is the dominant mode whether zonal wind or angular momentum is used in an EOF analysis, although the secondary EOFs are significantly different if you use angular momentum instead of zonal wind.
- The dominant mode appears with the same structure and with similar amplitude in all seasons and explains about 30% of the 10-day low-passed variance of zonal mean wind in all seasons.
- The temporal variability of the dominant mode of zonal wind is like that of Gaussian red noise with a one-day autocorrelation of about 0.8. Little evidence of bimodality or preferred periods can be seen, although the distribution is slightly skewed such that displacements of the jet toward lower latitudes are slightly larger and more long-lasting.
- Analysis of the momentum budget of the zonal flow vacillation indicates that the momentum driving by the transient eddies and associated meridional circulation is changed to support the zonal wind anomalies against surface drag and suggests that this feedback between the zonal flow and eddy forcing makes possible the large amplitude and temporal persistence of zonal wind variations.

- Correlation maps of the relative vorticity field show changes in composite eddy structure that occur in synchrony with the zonal flow vacillation. When the jet in the lower troposphere is displaced poleward, the eddy structures show evidence of enhanced equatorward propagation. When the jet is displaced equatorward, the eddy structures show less evidence of equatorward propagation and more evidence of eastward propagation as along a zonal waveguide.
- The eddy kinetic energy moves north and south with the jet in the lower troposphere. The zonal scale of the eddies remains about the same, so that the zonal wavenumber shifts to lower values when the jet is in higher latitudes.

In these results we see a strong confirmation in observations of results that have been obtained with idealized numerical models. As the dominant, equivalent-barotropic mode of zonal flow variation changes from one extreme to another, the zonal flow acceleration by transient eddies and the associated mean meridional circulation also changes so that the net advective forcing is very small in the free troposphere but large enough to offset large anomalies in frictional drag near the surface. In this way both extremes of the zonal flow vacillation can be balanced, nearly stationary states of the climate. In the structure of the eddies we also see some evidence of the development of a zonal waveguide when the jet is displaced equatorward. The similarity of some of these changes in eddy structure with idealized baroclinic life cycle experiments suggests that a much better understanding of the effect of zonal wind shear on baroclinic eddy life cycle development is worth pursuing. We also need to better understand the relative importance of the latitudinal displacements of the low-level jet and the change in zonal flow curvature at upper levels. Although these effects are easiest to diagnose in the Southern Hemisphere, it seems likely that the underlying dynamical processes also play a crucial role in the low-frequency variability of the more localized jets in the Northern Hemisphere.

Acknowledgments. We would like to thank David Lorenz for checking some of these results against the NCEP reanalysis. David Karoly, John Kidson, Ian Watterson, and the anonymous reviewers provided useful comments that improved the paper. This work was supported by the Climate Dynamics Division, National Science Foundation under Grant ATM-9313383.

REFERENCES

- Branstator, G., 1984: The relationship between zonal mean flow and quasi-stationary waves in the midtroposphere. *J. Atmos. Sci.*, **41**, 2163–2178.
- Davies, H. C., C. Schär, and H. Wernli, 1991: The palette of fronts and cyclones within a baroclinic wave development. *J. Atmos. Sci.*, **48**, 1666–1689.
- Dong, B. W., and I. N. James, 1997a: The effect of barotropic shear on baroclinic instability. 1. Normal mode problem. *Dyn. Atmos. Oceans*, **25**, 143–167.
- , and —, 1997b: The effect of barotropic shear on baroclinic instability. 2. The initial value problem. *Dyn. Atmos. Oceans*, **25**, 169–190.
- Edmon, H. J., Jr., B. J. Hoskins, and M. E. McIntyre, 1980: Eliassen–Palm cross sections for the troposphere. *J. Atmos. Sci.*, **37**, 2600–2616; Corrigendum, **38**, 1115.
- Feldstein, S. B., and W. A. Robinson, 1994: Comments on “Spatial structure of ultra-low frequency variability of the flow in a simple atmospheric circulation model”. *Quart. J. Roy. Meteor. Soc.*, **120**, 739–745.
- , and S. Lee, 1996: Mechanisms of zonal index variability in an aquaplanet GCM. *J. Atmos. Sci.*, **53**, 3541–3555.
- Gall, R. L., 1976: Structural change of growing baroclinic waves. *J. Atmos. Sci.*, **33**, 374–390.
- Hartmann, D.-L., 1995: A PV view of zonal flow vacillation. *J. Atmos. Sci.*, **52**, 2561–2576.
- , and P. Zuercher, 1998: Response of baroclinic life cycles to barotropic shear. *J. Atmos. Sci.*, **55**, 297–313.
- Held, I. M., 1975: Momentum transport by quasi-geostrophic eddies. *J. Atmos. Sci.*, **32**, 1494–1497.
- , and D. G. Andrews, 1983: On the direction of the eddy momentum flux in baroclinic instability. *J. Atmos. Sci.*, **40**, 2220–2231.
- Hoskins, B. J., I. N. James, and G. H. White, 1983: The shape, propagation and mean-flow interaction of large-scale weather systems. *J. Atmos. Sci.*, **40**, 1595–1612.
- James, I. N., 1987: Suppression of baroclinic instability in horizontally sheared flows. *J. Atmos. Sci.*, **44**, 3710–3720.
- , and P. M. James, 1992: Spatial structure of ultra-low-frequency variability of the flow in a simple atmospheric circulation model. *Quart. J. Roy. Meteor. Soc.*, **118**, 1211–1233.
- James, P. M., K. Fraedrich, and I. N. James, 1994: Wave-zonal flow interaction and ultra-low frequency variability of the flow in a simple atmospheric circulation model. *Quart. J. Roy. Meteor. Soc.*, **120**, 1045–1067.
- Karoly, D. J., 1990: The role of transient eddies in low-frequency zonal variations in the Southern Hemisphere circulation. *Tellus*, **42A**, 41–50.
- Kidson, J. W., 1988: Indices of the Southern Hemisphere zonal wind. *J. Climate*, **1**, 183–194.
- Lee, S., and S. Feldstein, 1996: Two types of wave breaking in an aquaplanet GCM. *J. Atmos. Sci.*, **53**, 842–857.
- Lo, F., 1996: Zonal flow vacillation: The interaction between eddies and the zonal mean flow. M.S. thesis, Department of Atmospheric Sciences, University of Washington, 72 pp.
- McIntyre, M. E., 1970: On the non-separable baroclinic parallel flow instability problem. *J. Fluid Mech.*, **40**, 273–306.
- Nakamura, M., and R. A. Plumb, 1994: The effects of flow asymmetry on the direction of Rossby wave breaking. *J. Atmos. Sci.*, **51**, 2031–2045.
- Nakamura, N., 1993: Momentum flux, flow symmetry, and the non-linear barotropic governor. *J. Atmos. Sci.*, **50**, 2159–2179.
- Nigam, S., 1990: On the structure of variability of the observed tropospheric and stratospheric zonal-mean wind. *J. Atmos. Sci.*, **47**, 1799–1813.
- North, G., T. Bell, R. Cahalan, and F. Moeng, 1982: Sampling errors in the estimation of empirical orthogonal functions. *Mon. Wea. Rev.*, **110**, 699–706.
- Peixoto, J. P., and A. H. Oort, 1992: *Physics of Climate*. American Institute of Physics, 520 pp.
- Pfeffer, R. L., 1987: Comparison of conventional and transformed Eulerian diagnostics in the troposphere. *Quart. J. Roy. Meteor. Soc.*, **113**, 237–254.
- Randel, W. J., 1990: Coherent wave–zonal flow interactions in the troposphere. *J. Atmos. Sci.*, **47**, 439–456.
- Rhines, P. B., 1975: Waves and turbulence on a β -plane. *J. Fluid Mech.*, **69**, 417–443.

- Robinson, W. A., 1991: The dynamics of the zonal index in a simple model of the atmosphere. *Tellus*, **43A**, 295–305.
- , 1996: Does eddy feedback sustain variability in the zonal index? *J. Atmos. Sci.*, **53**, 3556–3569.
- Rosby, C.-G., 1939: Relation between variations in the intensity of the zonal circulation of the atmosphere and the displacements of the semi-permanent centers of action. *J. Mar. Res.*, **2**, 38–55.
- Shiotani, M., 1990: Low-frequency variations of the zonal mean state of the Southern Hemisphere troposphere. *J. Meteor. Soc. Japan*, **68**, 461–470.
- Simmons, A. J., and B. J. Hoskins, 1980: Barotropic influences on the growth and decay of nonlinear baroclinic waves. *J. Atmos. Sci.*, **37**, 1679–1684.
- Thorncroft, C. D., B. J. Hoskins, and M. E. McIntyre, 1993: Two paradigms of baroclinic life-cycle behaviour. *Quart. J. Roy. Meteor. Soc.*, **119**, 17–55.
- Trenberth, K. E., 1984: Interannual variability of the Southern Hemisphere circulation: Representativeness of the year of the Global Weather Experiment. *Mon. Wea. Rev.*, **112**, 108–125.
- Wallace, J. M., and H.-H. Hsu, 1985: Another look at the index cycle. *Tellus*, **37A**, 478–486.
- Webster, P. J., and J. L. Keller, 1975: Atmospheric variations: Vacillations and index cycles. *J. Atmos. Sci.*, **32**, 1283–1300.
- Yoden, S., M. Shiotani, and I. Hirota, 1987: Multiple planetary flow regimes in the Southern Hemisphere. *J. Meteor. Soc. Japan*, **65**, 571–585.
- Yu, J.-Y., and D. L. Hartmann, 1993: Zonal flow vacillation and eddy forcing in a simple GCM of the atmosphere. *J. Atmos. Sci.*, **50**, 3244–3259.